A Thieno[3,4-b]thiophene-Based Non-fullerene Electron Acceptor for High-Performance Bulk-Heterojunction Organic Solar Cells

Feng Liu,[†,∥,‡] Zichun Zhou,[†,∥,‡] Cheng Zhang,[†,∥,‡] Thomas Vergote,[†] Haijun Fan,[†] Feng Liu,[*,§,⊥] and Xiaozhang Zhu[*,†,∥]

[†]Beijing National Laboratory for Molecular Sciences, CAS Key Laboratory of Organic Solids, Institute of Chemistry, Chinese Academy of Sciences, Beijing 100190, China
[§]Department of Physics and Astronomy, Shanghai Jiaotong University, Shanghai 200240, China
[∥]University of Chinese Academy of Sciences, Beijing 100049, China
[⊥]Materials Sciences Division, Lawrence Berkeley National Laboratory, Berkeley, California 94720, United States

S *Supporting Information*

ABSTRACT: A thieno[3,4-b]thiophene-based electron acceptor, ATT-1, is designed and synthesized. ATT-1 exhibits a planar conjugated framework, broad absorption with a large absorption coefficient, and a slightly high LUMO energy level. Bulk-heterojunction (BHJ) solar cells based on PTB7-Th electron donor and ATT-1 electron acceptor delivered power conversion efficiencies of up to 10.07%, which is among the best performances reported for non-fullerene BHJ solar cells using PTB7-Th as the electron donor.

Over the past two decades, bulk-heterojunction (BHJ) organic solar cells[1] have become a promising technology to utilize solar energy because of their flexibility, light weight, and low-cost roll-to-roll production. Generally, the active layer of BHJ solar cells consists of an electron donor and an electron acceptor that take a bicontinuous phase-separated morphology to convert light into electricity.[2] To date, most BHJ solar cells use fullerene derivatives as the electron acceptor and yield high power conversion efficiencies (PCEs) up to 10%,[3] owing to fullerene's high electron affinity and isotropic charge transport. However, fullerene acceptors have limitations, e.g., weak absorption of sunlight, poor morphological stability, high synthetic cost, and low tunability of the lowest unoccupied molecular orbital (LUMO) energy level. These issues led to a quick development of non-fullerene small-molecule acceptors,[4] which now show PCEs comparable to or even higher than those of fullerene-based BHJ devices.[5]

One of the most successful designs[6] for a photoactive material uses quinoidal resonance, extending the π-conjugation through the backbone, as seen in commercialized PTB7 or PTB7-Th polymers that are widely used in the development of high-performance solar cells.[7] Especially PTB7-Th has been used as a standard donor material for the screening of new non-fullerene acceptors.[5c,8] In our previous work, we extended this design by introducing strong donor–acceptor pairs to couple with quinoidal modulation,[9] e.g., combining a thieno[3,4-b]thiophene (TbT)[10]-rhodanine functional block with benzodithiophene. This molecular design (STB-n series shown in Scheme 1) has several distinct advantages, e.g., appropriate frontier energy

Scheme 1. Molecular Design of TbT-Based Non-fullerene Acceptor ATT-1
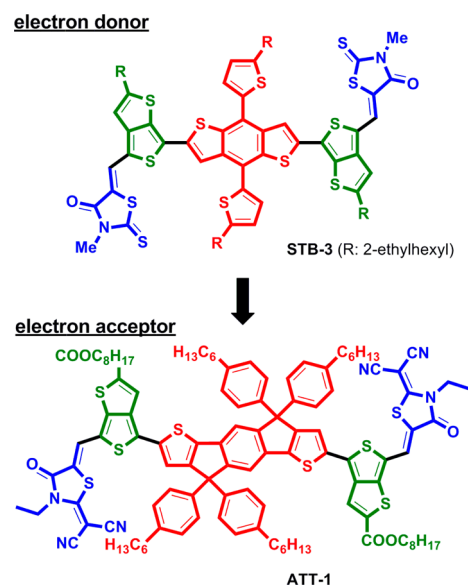
levels, better molecular planarity, large molecular π-surface to facilitate molecule–PCBM interaction, and high PCEs (9.26%).[11] We envisioned that the TbT-rhodanine functional block could be further used in designing acceptor materials whose energy levels can be readily tuned by coupling with new building blocks. A new non-fullerene acceptor, (Z)-dioctyl 6,6′-(4,4,9,9-tetrakis(4-hexylphenyl)-4,9-dihydro-s-indaceno[1,2-b:5,6-b′]dithiophene-2,7-diyl)bis(4-((Z)-(2-(dicyanomethylene)-3-ethyl-4-oxothiazolidin-5-ylidene)methyl)thieno-[3,4-b]thiophene-2-carboxylate), named as ATT-1, connecting TbT-rhodanine with the bulky indacenodithiophene (IDT) unit, is shown in Scheme 1. Instead of alkyl-substituted TbT and rhodanine in STB-3, ester-substituted TbT and 2-(1,1-dicyanomethylene)rhodanine, with stronger electron-withdrawing ability, were applied to simultaneously decrease the LUMO and highest occupied molecular orbital (HOMO) energy levels

## Scheme 2. Synthesis of Non-fullerene Acceptor ATT-1[a]
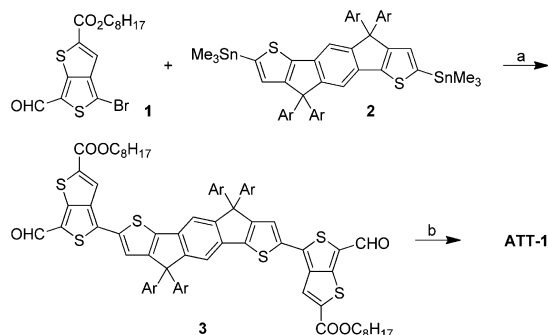
[a]Reagents and conditions: (a) Pd(PPh$_3$)$_4$, toluene/DMF, reflux; (b) 3-ethylrhodanine, β-alanine, dichloroethane/ethanol, 75 °C. Ar = *p*-hexylphenyl.

(Supporting Information (SI), Figure S1). ATT-1 possesses a planar conjugated framework, intense absorption ranging from 500 to 800 nm ($\varepsilon_{690nm} = 1.2 \times 10^5$ L mol^{-1} cm^{-1}), and a slightly high LUMO energy of −3.63 eV. The as-cast BHJ solar cells with PTB7-Th as the electron donor and ATT-1 as the electron acceptor exhibited PCEs up to 10.07%, which is among the highest efficiency for non-fullerene BHJ solar cells utilizing PTB7-Th as the donor material.[5c,8]

As shown in Scheme 2, ATT-1 was synthesized by a simple two-step method: a Stille-type cross-coupling reaction between octyl 4-bromo-6-formylthieno[3,4-*b*]thiophene-2-carboxylate **1**[10] and (4,4,9,9-tetrakis(4-hexylphenyl)-4,9-dihydro-s-indaceno[1,2-*b*:5,6-*b'*]dithiophene-2,7-diyl)bis(trimethyl-stannane) **2**[12] to generate dialdehyde **3**, followed by a Knoevenagel condensation with 2-(3-ethyl-4-oxothiazolidin-2-ylidene)malononitrile to afford ATT-1 in 76% yield. The solubility of ATT-1 is quite good in halogenated solvents, e.g., chloroform, chlorobenzene, and *o*-dichlorobenzene. According to thermogravimetric analysis, ATT-1 exhibits high thermal stability (5% weight loss at 320 °C; SI, Figure S2). An ATT-1 chloroform solution shows intense absorption in the 500−800 nm region, with a large molar absorption coefficient of 1.2×10^5 L mol^{-1} cm^{-1} at 690 nm (Figure 1a). ATT-1 thin film exhibits a
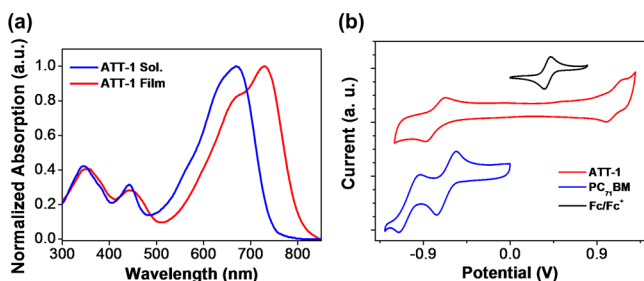
Figure 1. (a) Normalized UV/vis absorption spectra of ATT-1 in chloroform and in thin film. (b) Cyclic voltammograms of ATT-1 and PC$_{71}$BM.

maximum absorption peak at 736 nm, which is bathochromically shifted by 46 nm. Noted that the maximum photon flux density of sunlight is around 700 nm, so the strong and broad absorption of ATT-1 could enhance the short-circuit current (J_{sc}) in photovoltaic devices. The optical bandgap of ATT-1 is determined to be 1.54 eV according to the thin-film absorption onset. According to the cyclic voltammetry measurements (Figure 1b), the HOMO and LUMO energy levels are estimated

to be −5.50 and −3.63 eV, respectively (Figure 1b), using $E_{HOMO/LUMO} = -(4.80 + E_{ox/red}^{1/2})$ eV. The LUMO energy level of ATT-1 is slightly higher than that of PC$_{71}$BM (−3.75 eV), which is beneficial to achieving high open-circuit voltage (V_{oc}).[13]

For a feasible comparison of the performance of PC$_{71}$BM- and ATT-1-based solar cells, we applied a conventional BHJ device structure of ITO/PEDOT:PSS/PTB7-Th:ATT-1/PFN/Al. The optimized active layers with a thickness of 130 nm were formed by spin-coating from a chlorobenzene solution of PTB7-Th:ATT-1 (1:1.5 weight ratio, 25 mg/mL in total weight concentration). As indicated in Table 1, the PCE values

Table 1. Device Performance of BHJ Organic Solar Cells Based on PTB7-Th:ATT-1 and PTB7-Th:P$_{71}$BM (Both 1:1.5 Weight Ratio) under AM 1.5G Illumination, 100 mW cm^{-2}

acceptor	thickness (nm)	V_{oc} (V)	J_{sc} (mA cm^{-2})	FF (%)	PCE (%)[a]
ATT-1	130	0.92	12.29	39	4.46 (4.39)
ATT-1[b]	100	0.88	16.18	68	9.78 (9.67)
ATT-1[b]	130	0.87	16.48	70	10.07 (9.89)
ATT-1[b]	160	0.87	16.41	66	9.59 (9.43)
PC$_{71}$BM[c]	100	0.79	16.62	67	9.02 (8.85)
PC$_{71}$BM[c]	130	0.78	16.03	67	8.46 (8.22)

[a]Average PCEs in parentheses for 24 devices. [b]1% DIO is added. [c]3% DIO is added.

dramatically increase from 4.46% to 10.07% when 1% (v/v) 1,8-diiodooctane (DIO) is applied as the processing additive, which leads to increased J_{sc} and fill factor (FF) (12.29 vs 16.48 mA cm^{-2} and 0.39 vs 0.70 without and with DIO presented in devices, respectively, Figure 2b). The ATT-1-based solar cells exhibit higher V_{oc} and FF than those based on PC$_{71}$BM acceptor (0.87 vs 0.79 eV and 0.70 vs 0.67 in devices; SI, Figure S3) with comparable J_{sc}. External quantum efficiency (EQE) curves are shown in Figure 2c. The J_{sc} value is calculated to be 15.8 mA cm^{-2} according to the EQE curve, which agrees well with those from photovoltaic *J*−*V* test (~4% error). Thus, the PCEs of PTB7-Th and ATT-1-based solar cells are comparable to, if not better than, those of the state-of-the-art BHJ solar cells using PC$_{71}$BM.

The influence of DIO on charge generation and extraction is investigated by measuring the photocurrent density (J_{ph}) versus the internal voltage (V_{in}) (Figure 2d) and the dependence of the J_{sc} on illumination intensity (Figure 2e). J_{ph} is defined as $J_L - J_D$, where J_L and J_D are the current density under illumination and in the dark, respectively. V_{in} is calculated by $V_0 - V$.[14] As shown in Figure 2d, J_{ph} of the blend film without DIO does not saturate, even at high V_{in} (>1.5 V), indicating that the charge extraction in the solar cell is quite poor. Meanwhile, J_{ph} of the blend film using 1% DIO increases dramatically at low V_{in} and saturates promptly at $V_{in} \approx 0.3$ V. Thus, the corresponding short-circuit voltage falls within the saturation regime, and the saturation current density (J_{sat}) is 16.83 mA cm^{-2}. The high J_{ph}/J_{sat} values under the short-circuit condition and maximum power points are 0.98 and 0.82, indicating efficient exciton dissociation in the system of PTB7-Th:ATT-1. The dependence of J_{sc} on illumination intensity is also measured to study the recombination kinetics.[15] If the slope of the J_{sc} vs illumination curve approaches 1, the bimolecular recombination can be neglected, and the free carriers can be collected effectively. In Figure 2e, the slopes for the blend film with and without DIO are 0.94 and 0.87, respectively, indicating that strong bimolecular recombination can be suppressed when DIO is introduced. Consequently, efficient charge generation,
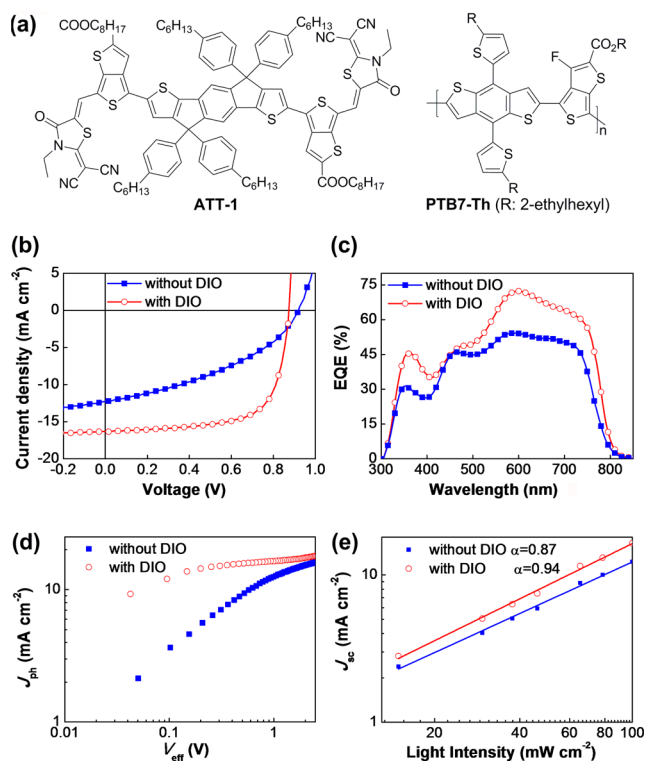
Figure 2. (a) Chemical structures of non-fullerene acceptor ATT-1 and polymer donor PTB7-Th. (b) Characteristic current density vs voltage ($J–V$) curves of the PTB7-Th:ATT-1-based solar cells without (blue line) and with (red line) solvent additive DIO (1%, v/v) under AM 1.5G irradiation (100 mW cm^{-2}). (c) EQE curves of the corresponding solar cells. (d) $J_{ph}–V_{eff}$ characteristics. (e) Double-logarithmic plots of J_{sc} as a function of incident light intensity.

extraction, and weak recombination give rise to the improved J_{sc} after addition of 1% DIO.

Charge-transport properties were investigated by the space charge-limited current (SCLC) method using hole- and electron-only devices (SI, Figure S4). The hole and electron mobilities of the blend film without DIO are determined to be 0.58 × 10^{-4} and 0.25 × 10^{-4} cm^2 V^{-1} s^{-1}, respectively. After addition of 1% DIO, the hole and electron mobilities are increased to 5.13 × 10^{-4} and 2.40 × 10^{-4} cm^2 V^{-1} s^{-1}, respectively. The 10-fold increase of hole and electron mobilities is responsible for the improved FFs in devices.

To understand the excellent device performance of the PTB7-Th:ATT-1 blend, we used grazing incidence X-ray diffraction (GIXD) and resonant soft X-ray scattering (RSoXS) to investigate the microstructures of the neat and blend thin films.[16] The two-dimensional (2D) GIXD patterns and the corresponding line-cuts of neat PTB7-Th, neat ATT-1, and their blends with and without DIO are shown in Figure 3. PTB7-Th showed a (100) diffraction peak in the in-plane (IP) direction at 0.27 Å^{-1} and a (010) diffraction peak in the out-of-plane (OOP) direction at 1.63 Å^{-1}. The corresponding inter-lamellae spacings are 22.4 and 3.85 Å, and the polymer crystalline regime takes preferential face-on orientation as seen from enhanced π–π stacking diffraction in OOP direction.[17] The neat film of ATT-1 exhibits a broad alkyl-stacking peak at 0.34 Å with no azimuthal dependence, which corresponds to the inter-lamellae spacing of 18.5 Å. The neat film of ATT-1 shows a diffusive diffraction arc around 1.26 Å^{-1} and a broad π–π stacking peak at 1.75 Å^{-1},
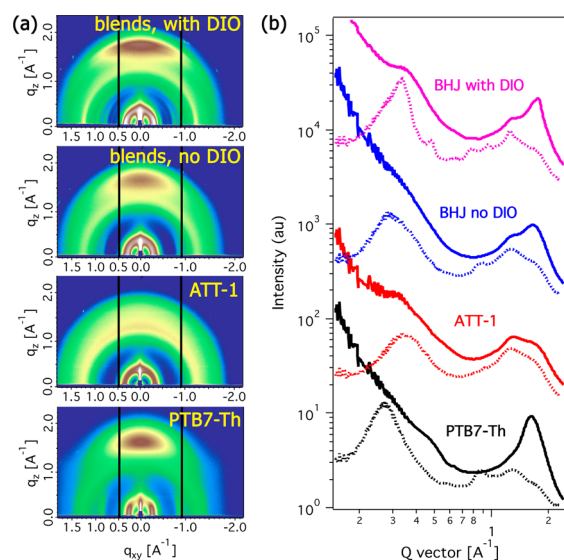
Figure 3. (a) 2D GIXD diffraction images of the pristine and PTB7-Th:ATT-1 blend films. (b) IP (dotted line) and OOP (solid line) X-ray scattering profiles extracted from the 2D GIXD images.

corresponding to π–π stacking distance of 3.58 Å. The blend film without DIO shows combined diffraction features of PTB7-Th and ATT-1. The alkyl–alkyl packing region and π–π stacking region are combined features from both components and appear as broad peaks that cannot be easily separated. Peak-splitting fitting of the 0.2–0.5 Å^{-1} region yields PTB7-Th and ATT-1 crystal sizes of 7.2 and 4.1 nm, respectively. In DIO-processed blends, enhanced diffraction features from ATT-1 are seen in both alkyl–alkyl packing and π–π stacking regions. The crystal sizes of (100) for PTB7-Th and ATT-1 are 7.4 and 10.2 nm. Thus, DIO strongly enhanced ATT-1 crystallization. The π–π stacking peak region cannot be easily fitted. However, the sharper peak at 1.70 Å^{-1} in the OOP direction indicated that both PTB7-Th and ATT-1 intermolecular stacking were enhanced. We scaled IP and OOP profiles and normalized around the 1–1.2 Å^{-1} amorphous region signal (SI, Figure S6). More intense π–π stacking features were seen in the OOP region; thus, face-on orientation dominates. These characteristics of the increased crystal sizes and preferential face-on orientation lead to improved charge transport in DIO-processed thin films.

RSoXS is used to investigate the phase separation of PTB7-Th:ATT-1 blend films. A photon energy of 285.2 eV was used by employing enhanced contrast at the carbon K-edge. As indicated in SI, Figure S7, the PTB7-Th:ATT-1 blend with no DIO treatment shows weak scattering features with a broad hump located at around 0.01 Å^{-1}, giving a size scale of ~60 nm for phase separation. PTB7-Th and ATT-1 are both conjugated materials of similar components, and the scattering contrast is low.[18] A weak scattering signal indicates that these molecules mix well. This feature leads to poor carrier extraction and low FF in devices. DIO additive helps to improve the thin-film morphology, and in RSoXS, enhanced scattering intensity across a broad q region from 0.04 to 0.2 Å^{-1} was seen, and thus a broad length scale of phase separation (30–150 nm). The enhanced phase separation and crystallinity in the blended thin film give rise to a mobility jump for both electrons and holes, leading to dramatically increased FFs and PCEs. Thus, a proper morphological optimization is critical in exploring the potential of new OPV materials.

In summary, a new electron acceptor, ATT-1, based on a T*b*T-rhodanine building block has been designed and synthesized. ATT-1 exhibits broad absorption, with a large absorption coefficient and suitable LUMO energy level. BHJ solar cells based on PTB7-Th donor and ATT-1 acceptor delivered high PCEs of up to 10.07%, which is among the highest for non-fullerene BHJ solar cells using PTB7-Th as the electron donor. To our knowledge, ATT-1 is the first T*b*T-based non-fullerene acceptor. The proper energy level alignment, excellent carrier transport property, and proper morphology in ATT-1-based BHJ blends advocate for its promising future in OPV applications.

■ ASSOCIATED CONTENT

Ⓢ Supporting Information

The Supporting Information is available free of charge on the ACS Publications website at DOI: 10.1021/jacs.6b08523.

Experimental details, DFT calculations, TGA and SCLC measurements, AFM images, and NMR spectra (PDF)

■ AUTHOR INFORMATION

Corresponding Authors

*fengliu82@sjtu.edu.cn
*xzzhu@iccas.ac.cn

ORCID Ⓘ

Xiaozhang Zhu: 0000-0002-6812-0856

Author Contributions

‡F.L., Z.Z., and C.Z. contributed equally.

Notes

The authors declare no competing financial interest.

■ ACKNOWLEDGMENTS

■ REFERENCES

(1) (a) Brabec, C.; Scherf, U.; Dyakonov, V. *Organic Photovoltaics: Materials, Device Physics, and Manufacturing Technologies*, 2nd ed.; Wiley-VCH Verlag GmbH & Co. KGaA: Weinheim, Germany, 2014. (b) Lu, L.; Zheng, T.; Wu, Q.; Schneider, A. M.; Zhao, D.; Yu, L. *Chem. Rev.* **2015**, *115*, 12666. (c) Dou, L.; You, J.; Hong, Z.; Xu, Z.; Li, G.; Street, R. A.; Yang, Y. *Adv. Mater.* **2013**, *25*, 6642.

(2) Yu, G.; Gao, J.; Hummelen, J. C.; Wudl, F.; Heeger, A. J. *Science* **1995**, *270*, 1789.

(3) (a) Zhao, J.; Li, Y.; Yang, G.; Jiang, K.; Lin, H.; Ade, H.; Ma, W.; Yan, H. *Nature Energy* **2016**, *1*, 15027. (b) Zhang, S.; Ye, L.; Zhao, W.; Yang, B.; Wang, Q.; Hou, J. *Sci. China: Chem.* **2015**, *58*, 248. (c) Vohra, V.; Kawashima, K.; Kakara, T.; Koganezawa, T.; Osaka, I.; Takimiya, K.; Murata, H. *Nat. Photonics* **2015**, *9*, 403. (d) Kan, B.; Zhang, Q.; Li, M.; Wan, X.; Ni, W.; Long, G.; Wang, Y.; Yang, X.; Feng, H.; Chen, Y. *J. Am. Chem. Soc.* **2014**, *136*, 15529.

(4) (a) Lin, Y.; Zhan, X. *Mater. Horiz.* **2014**, *1*, 470. (b) Nielsen, C. B.; Holliday, S.; Chen, H.-Y.; Cryer, S.; McCulloch, I. *Acc. Chem. Res.* **2015**, *48*, 2803.

(5) (a) Zheng, Z.; Zhang, S.; Zhang, J.; Qin, Y.; Li, W.; Yu, R.; Wei, Z.; Hou, J. *Adv. Mater.* **2016**, *28*, 5133. (b) Lin, Y.; He, Q.; Zhao, F.; Huo, L.; Mai, J.; Lu, X.; Su, C.-J.; Li, T.; Wang, J.; Zhu, J.; Sun, Y.; Wang, C.; Zhan, X. *J. Am. Chem. Soc.* **2016**, *138*, 2973. (c) Lin, Y.; Zhao, F.; He, Q.; Huo, L.; Wu, Y.; Parker, T. C.; Ma, W.; Sun, Y.; Wang, C.; Zhu, D.; Heeger, A. J.; Marder, S. R.; Zhan, X. *J. Am. Chem. Soc.* **2016**, *138*, 4955. (d) Meng, D.; Sun, D.; Zhong, C.; Liu, T.; Fan, B.; Huo, L.; Li, Y.; Jiang, W.; Choi, H.; Kim, T.; Kim, J. Y.; Sun, Y.; Wang, Z.; Heeger, A. J. *J. Am. Chem. Soc.* **2016**, *138*, 375. (e) Holliday, S.; Ashraf, R. S.; Wadsworth, A.; Baran, D.; Yousaf, S. A.; Nielsen, C. B.; Tan, C.-H.; Dimitrov, S. D.; shang, Z.; Gasparini, N.; Alamoudi, M.; Laquai, F.; Brabec, C. J.; Salleo, A.; Durrant, J. R.; McCulloch, I. *Nat. Commun.* **2016**, *7*, 11585. (f) Meng, D.; Fu, H.; Xiao, C.; Meng, X.; Winands, T.; Ma, W.; Wei, W.; Fan, B.; Huo, L.; Doltsinis, N. L.; Li, Y.; Sun, Y.; Wang, Z. *J. Am. Chem. Soc.* **2016**, *138*, 10184. (g) Liu, J.; Chen, S.; Qian, D.; Gautam, B.; Yang, G.; Zhao, J.; Bergqvist, J.; Zhang, F.; Ma, W.; Ade, H.; Inganäs, O.; Gundogdu, K.; Gao, G.; Yan, H. *Nature Energy* **2016**, *1*, 16089.

(6) (a) Lu, L.; Yu, L. *Adv. Mater.* **2014**, *26*, 4413. (b) Liang, Y.; Yu, L. *Acc. Chem. Res.* **2010**, *43*, 1227.

(7) Selected examples: (a) Page, Z. A.; Liu, Y.; Duzhko, V. V.; Russell, T. P.; Emrick, T. *Science* **2014**, *346*, 441. (b) Ouyang, X.; Peng, R.; Ai, L.; Zhang, X.; Ge, Z. *Nat. Photonics* **2015**, *9*, 520. (c) He, Z.; Zhong, C.; Su, S.; Xu, M.; Wu, H.; Cao, Y. *Nat. Photonics* **2012**, *6*, 591. (d) Lu, L.; Xu, T.; Chen, W.; Landry, E. S.; Yu, L. *Nat. Photonics* **2014**, *8*, 716. (e) He, Z.; Xiao, B.; Liu, F.; Wu, H.; Yang, Y.; Xiao, S.; Wang, C.; Russell, T. P.; Cao, Y. *Nat. Photonics* **2015**, *9*, 174.

(8) (a) Zhong, H.; Wu, C.-H.; Li, C.-Z.; Carpenter, J.; Chueh, C.-C.; Chen, U.-Y.; Ade, H.; Jen, A. K.-Y. *Adv. Mater.* **2016**, *28*, 951. (b) Wu, Q.; Zhao, D.; Schneider, A. M.; Chen, W.; Yu, L. *J. Am. Chem. Soc.* **2016**, *138*, 7248. (c) Zhong, Y.; Trinh, M. T.; Chen, R.; Purdum, G. E.; Khlyabich, P. P.; Sezen, M.; Oh, S.; Zhu, H.; Fowler, B.; Zhang, B.; Wang, W.; Nam, C.-Y.; Sfeir, M. Y.; Black, C. T.; Steigerwald, M. L.; Loo, Y.-L.; Ng, F.; Zhu, X.-Y.; Nuckolls, C. *Nat. Commun.* **2015**, *6*, 8242. (d) Hwang, Y.-J.; Li, H.; Courtright, B. A. E.; Subramaniyan, S.; Jenekhe, S. A. *Adv. Mater.* **2016**, *28*, 124. (e) Lin, Y.; Wang, J.; Zhang, Z.-G.; Bai, H.; Li, Y.; Zhu, D.; Zhan, X. *Adv. Mater.* **2015**, *27*, 1170. (f) Lin, Y.; Zhang, Z.-G.; Bai, H.; Wang, J.; Yao, Y.; Li, Y.; Zhu, D.; Zhan, X. *Energy Environ. Sci.* **2015**, *8*, 610. (g) Hwang, Y.-J.; Courtright, B. A. E.; Ferreira, A. S.; Tolbert, S. H.; Jenekhe, S. A. *Adv. Mater.* **2015**, *27*, 4578. (h) Jung, J. W.; Jo, J. W.; Chueh, C.-C.; Liu, F.; Jo, W. H.; Russell, T. P.; Jen, A. K.-Y. *Adv. Mater.* **2015**, *27*, 3310.

(9) (a) Zhang, C.; Li, H.; Wang, J.; Zhang, Y.; Qiao, Y.; Huang, D.; Di, C.-a.; Zhan, X.; Zhu, X.; Zhu, D. *J. Mater. Chem. A* **2015**, *3*, 11194. (b) Liu, F.; Fan, H.; Zhang, Z.; Zhu, X. *ACS Appl. Mater. Interfaces* **2016**, *8*, 3661.

(10) Liu, F.; Espejo, G. L.; Qiu, S.; Oliva, M. M.; Pina, J.; de Melo, J. S. S.; Casado, J.; Zhu, X. *J. Am. Chem. Soc.* **2015**, *137*, 10357.

(11) Xu, S.; Zhou, Z.; Fan, H.; Ren, L.; Liu, F.; Zhu, X.; Russell, T. P. *J. Mater. Chem. A* **2016**, *4*, 17354.

(12) Zhang, C.; Zang, Y.; Gann, E.; McNeill, C. R.; Zhu, X.; Di, C.-a.; Zhu, D. *J. Am. Chem. Soc.* **2014**, *136*, 16176.

(13) He, Y.; Chen, H.-Y.; Hou, J.; Li, Y. *J. Am. Chem. Soc.* **2010**, *132*, 1377.

(14) Blom, P. W. M.; Mihailetchi, V. D.; Koster, L. J. A.; Markov, D. E. *Adv. Mater.* **2007**, *19*, 1551.

(15) (a) Riedel, I.; Parisi, J.; Dyakonov, V.; Lutsen, L.; Vanderzande, D.; Hummelen, J. *Adv. Funct. Mater.* **2004**, *14*, 38. (b) Cowan, S. R.; Roy, A.; Heeger, A. J. *Phys. Rev. B: Condens. Matter Mater. Phys.* **2010**, *82*, 245207.

(16) (a) Vandewal, K.; Himmelberger, S.; Salleo, A. *Macromolecules* **2013**, *46*, 6379. (b) Rivnay, J.; Mannsfeld, S. C. B.; Miller, C. E.; Salleo, A.; Toney, M. F. *Chem. Rev.* **2012**, *112*, 5488.

(17) Baker, J. L.; Jimison, L. H.; Mannsfeld, S.; Volkman, S.; Yin, S.; Subramanian, V.; Salleo, A.; Alivisatos, A. P.; Toney, M. F. *Langmuir* **2010**, *26*, 9146.

(18) (a) Lin, H.; Chen, S.; Li, Z.; Lai, J. Y. L.; Yang, G.; McAfee, T.; Jiang, K.; Li, Y.; Liu, Y.; Hu, H.; Zhao, J.; Ma, W.; Yan, H.; Ade, H. *Adv. Mater.* **2015**, *27*, 7299. (b) Collins, B. A.; Li, Z.; Tumbleston, J. R.; Gann, E.; McNeill, C. R.; Ade, H. *Adv. Energy Mater.* **2013**, *3*, 65.